Article

Current Biology

Dissociable oscillatory theta signatures of memory formation in the developing brain

Highlights

- Pediatric ECoG reveals how key memory regions interact during memory formation
- Slow and fast theta frequencies differentiate by age in a double dissociation
- Medial temporal and prefrontal regions are coupled through distinct mechanisms
- Strengthened coupling and cingulum tract integrity predict age-related memory gains

Authors

Elizabeth L. Johnson, Qin Yin, Nolan B. O'Hara, Lingfei Tang, Jeong-Won Jeong, Eishi Asano, Noa Ofen

Correspondence

eljohnson@northwestern.edu (E.L.J.), noa.ofen@wayne.edu (N.O.)

In brief

Johnson et al. test interactions among key brain regions during memory formation using pediatric subdural recording. The medial temporal lobe and prefrontal cortex are coupled through distinct slow and fast theta mechanisms, which differentiate in frequency by age. Strengthened coupling and cingulum tract integrity predict age-related memory gains.

Johnson et al., 2022, Current Biology *32*, 1–13
April 11, 2022 © 2022 Elsevier Inc.
https://doi.org/10.1016/j.cub.2022.01.053

CellPress

Please cite this article in press as: Johnson et al., Dissociable oscillatory theta signatures of memory formation in the developing brain, Current Biology (2022), https://doi.org/10.1016/j.cub.2022.01.053

Current Biology

CellPress

Article

Dissociable oscillatory theta signatures of memory formation in the developing brain

Elizabeth L. Johnson,[1,2,3,7,*] Qin Yin,[1,4] Nolan B. O'Hara,[5] Lingfei Tang,[1,4] Jeong-Won Jeong,[5,6] Eishi Asano,[5,6] and Noa Ofen[1,4,5,*]

[1]Life-Span Cognitive Neuroscience Program, Institute of Gerontology and Merrill Palmer Skillman Institute, Wayne State University, Detroit, MI 48202, USA
[2]Departments of Medical Social Sciences and Pediatrics, Northwestern University, Chicago, IL 60611, USA
[3]Helen Wills Neuroscience Institute, University of California, Berkeley, Berkeley, CA 94720, USA
[4]Department of Psychology, Wayne State University, Detroit, MI 48202, USA
[5]Translational Neuroscience Program, Wayne State University, Detroit, MI 48201, USA
[6]Departments of Pediatrics and Neurology, Children's Hospital of Michigan, Wayne State University, Detroit, MI 48201, USA
[7]Lead contact
*Correspondence: eljohnson@northwestern.edu (E.L.J.), noa.ofen@wayne.edu (N.O.)
https://doi.org/10.1016/j.cub.2022.01.053

SUMMARY

Understanding complex human brain functions is critically informed by studying such functions during development. Here, we addressed a major gap in models of human memory by leveraging rare direct electrophysiological recordings from children and adolescents. Specifically, memory relies on interactions between the medial temporal lobe (MTL) and prefrontal cortex (PFC), and the maturation of these interactions is posited to play a key role in supporting memory development. To understand the nature of MTL-PFC interactions, we examined subdural recordings from MTL and PFC in 21 neurosurgical patients aged 5.9–20.5 years as they performed an established scene memory task. We determined signatures of memory formation by comparing the study of subsequently recognized to forgotten scenes in single trials. Results establish that MTL and PFC interact via two distinct theta mechanisms, an ~3-Hz oscillation that supports amplitude coupling and slows down with age and an ~7-Hz oscillation that supports phase coupling and speeds up with age. Slow and fast theta interactions immediately preceding scene onset further explained age-related differences in recognition performance. Last, with additional diffusion imaging data, we linked both functional mechanisms to the structural maturation of the cingulum tract. Our findings establish system-level dynamics of memory formation and suggest that MTL and PFC interact via increasingly dissociable mechanisms as memory improves across development.

INTRODUCTION

Episodic memory, the ability to form and retrieve explicit memories, is fundamental to human experience and shows robust improvement over a protracted developmental trajectory from childhood into young adulthood.[1–7] Development of this fundamental ability occurs concomitant with the protracted maturation of key brain regions, including the medial temporal lobe (MTL), prefrontal cortex (PFC), and tracts connecting MTL and PFC.[8–12] The MTL is critical to episodic memory and supports memory formation in children, whereas increased PFC involvement supports improved memory across development.[13,14] These well-documented observations are consistent with a two-component model of memory development: associative processes relying on MTL are theorized to mature earlier than control processes relying on PFC.[1,3,15–17] By such a model, neural indices of memory formation increasingly implicate PFC to benefit memory performance as children mature into adulthood. Indeed, extant data link increased co-activation of MTL and PFC, as indexed by correlated fMRI hemodynamic responses, to developmental gains in memory.[13,18–21] Performance gains are thus posited to result from a maturing dialog between MTL and PFC, although how this occurs is unknown. The neurophysiological mechanisms of MTL-PFC interactions during memory formation have not been examined in the developing brain.

We address this gap by conducting a systematic investigation of MTL-PFC interactions during memory formation using rare subdural recordings from pediatric neurosurgical patients (10 females and 11 males aged 5.9–20.5 years; Table S1) and structural imaging of white matter tracts available from a subset of patients. All patients were diagnosed with epilepsy and being monitored invasively as part of seizure management (see Table S1 for individual seizure information). Based on extensive literature in adults and animal models,[22–36] we hypothesized that neural oscillations in the theta band (2–8 Hz) would provide the functional infrastructure for MTL-PFC interactions during memory formation in the developing brain. Neural oscillations provide optimal windows for regional excitability and inter-regional coordination.[37] In MTL, oscillations in the theta band are ubiquitous and support neuronal computations underlying associative

Please cite this article in press as: Johnson et al., Dissociable oscillatory theta signatures of memory formation in the developing brain, Current Biology (2022), https://doi.org/10.1016/j.cub.2022.01.053

processes of information integration.[38] Theta oscillations further coordinate MTL and PFC and permit communication and information transfer between regions.[39–41] We predicted that theta oscillations would coordinate MTL-PFC interactions during memory formation in children. Likewise, age-related differences in memory performance would reflect age-related differences in MTL-PFC interactions.

To test these predictions, we analyzed electrocorticography (ECoG) data recorded during the performance of an established task of recognition memory for visual scenes.[6,14,18,42–47] ECoG affords multiple advantages over noninvasive measures, including millisecond temporal and millimeter spatial resolution and high signal-to-noise ratio enabling single-trial precision, and thus provides a powerful tool in the study of human memory.[6,22,27] The aims were 3-fold. First, we determined signatures of memory formation by comparing trial-by-trial data from the study phase based on subsequent memory at test, as is recommended for developmental research to control for factors not directly related to memory formation.[1,6] Second, we identified the signatures of memory formation that explain inter-individual age-related differences in recognition performance.[6] Third, we mapped individual function to structure by correlating the memory formation signatures that explain age-related performance differences with the integrity of white matter tracts connecting MTL and PFC.

We took an iterative, data-driven approach by refining specific hypotheses to reflect specific discoveries about the neurophysiology and neuroanatomy of the developing brain. Accordingly, we first demonstrated typical memory development in our patient sample through analyses of behavioral performance, ECoG signals within MTL and PFC, and structural tracts connecting MTL and PFC.[6,27] Next, based on the discovery of age-related differences in oscillatory theta frequencies within MTL and PFC, we systematically investigated MTL-PFC interactions while controlling for inter-individual differences in theta frequencies. Finally, we linked the signatures of memory formation that explain inter-individual differences in recognition performance to the structural development of the brain. Our findings establish that theta oscillations provide the functional infrastructure for MTL-PFC interactions in the human brain and suggest that MTL and PFC interact via increasingly dissociable slow and fast theta mechanisms as memory improves across development.

RESULTS

Typical trajectory of memory development

Subjects studied sets of 40 visual scenes and verbalized a semantic judgment of whether each scene was indoor or outdoor in preparation for a recognition memory test of all scenes presented at study intermixed with 20 new scenes as foils (Figure 1A). We first confirmed that subjects were proficient at the scene-encoding task (rate of correct indoor/outdoor responses: mean ± SD, 0.94 ± 0.05; chance, 0.5; Table S1). To control for attention at study, trials with incorrect indoor/outdoor responses were excluded from all further analysis.[42,43] Of studied scenes with correct indoor/outdoor responses, a mean of 0.67 were correctly identified as old (i.e., hit), and the remaining 0.33 were incorrectly identified as new (miss; SD, 0.17). Of scenes used as foils at recognition, a mean of 0.69 were correctly identified as new, and the remaining 0.31 were incorrectly identified as old (false alarm; SD, 0.18). Recognition performance (hit rate − false alarm rate) varied across subjects from 0.02 to 0.76 (mean ± SD, 0.37 ± 0.21; Table S1).

Performance was positively correlated with age ($r = 0.30$; 95% CI 0.02–0.62) supported by a Bayes Factor (BF_{10}) of 1.08. As shown in Figure 1B, inter-individual variability attenuated the strength of the relationship between performance and age and was particularly apparent among adolescents aged 15–17 years. Critically, however, these patterns replicate the typical developmental trajectory of performance on this scene memory task (Figure S1A). Previous research in large non-clinical samples has consistently demonstrated modest positive relationships between performance and age in children and adolescents, with marked variability among adolescents.[6,14,18,44–46] More robust relationships have been reported in investigations that subdivided individual data based on stimulus and response criteria (e.g., scene complexity, recognition confidence) with consistent outcomes in ECoG[43] and non-clinical samples.[45] Thus, we show that these data reflect typical memory development and, in the second study aim, identify ECoG signatures of memory formation that differentiate top performing adolescents from both lower performing adolescents and children.

Medial temporal spectral signatures of memory formation

ECoG signals were recorded from MTL (i.e., parahippocampal and rhinal cortices), yielding 80 artifact-free and nonpathologic electrodes across 21 subjects (mean ± SD, 4 ± 2 electrodes/subject). Simultaneous PFC recording yielded 357 artifact-free and nonpathologic electrodes across 20 of 21 subjects in the MTL sample (18 ± 9 electrodes/subject). PFC coverage included the inferior frontal gyrus (IFG) in 16 subjects aged 5.9–19.4 years, middle frontal gyrus (MFG) in 20 subjects aged 5.9–20.5 years, and superior frontal gyrus (SFG) in 14 subjects aged 5.9–20.5 years. Group-level coverage is shown in Figure 1C, and individual coverage information is provided in Table S1. For each region, we analyzed activity during memory formation (i.e., subsequent hit trials) and failure of memory formation (i.e., subsequent miss trials) across the full power spectrum. A time-frequency representation of power for each study trial was computed from 1.5 to 250 Hz, and event-related activity was quantified using statistical bootstrapping.[42,43] To identify signatures of memory formation, individual subsequent hit- and miss-trial outputs were averaged across electrodes within a region and submitted to permutation testing with cluster-based correction for multiple comparisons.[48]

We first determined spectral signatures of memory formation in MTL by comparing activity during the encoding of subsequently recognized relative to forgotten scenes (i.e., subsequent memory analysis[1,6]). This contrast revealed a large cluster of lower power during successful memory formation (i.e., negative subsequent memory effects; $p = 0.004$). Effects were identified between 2.5 and 10.4 Hz and spanned 0.79 to 2.62 s from scene onset. As shown in Figure 2, effects from 2.5–4.3 Hz preceded the mean indoor/outdoor encoding task response and effects from 5.2–10.4 Hz extended post-response. These subsequent memory effects implicate the theta band and are consistent

Please cite this article in press as: Johnson et al., Dissociable oscillatory theta signatures of memory formation in the developing brain, Current Biology (2022), https://doi.org/10.1016/j.cub.2022.01.053

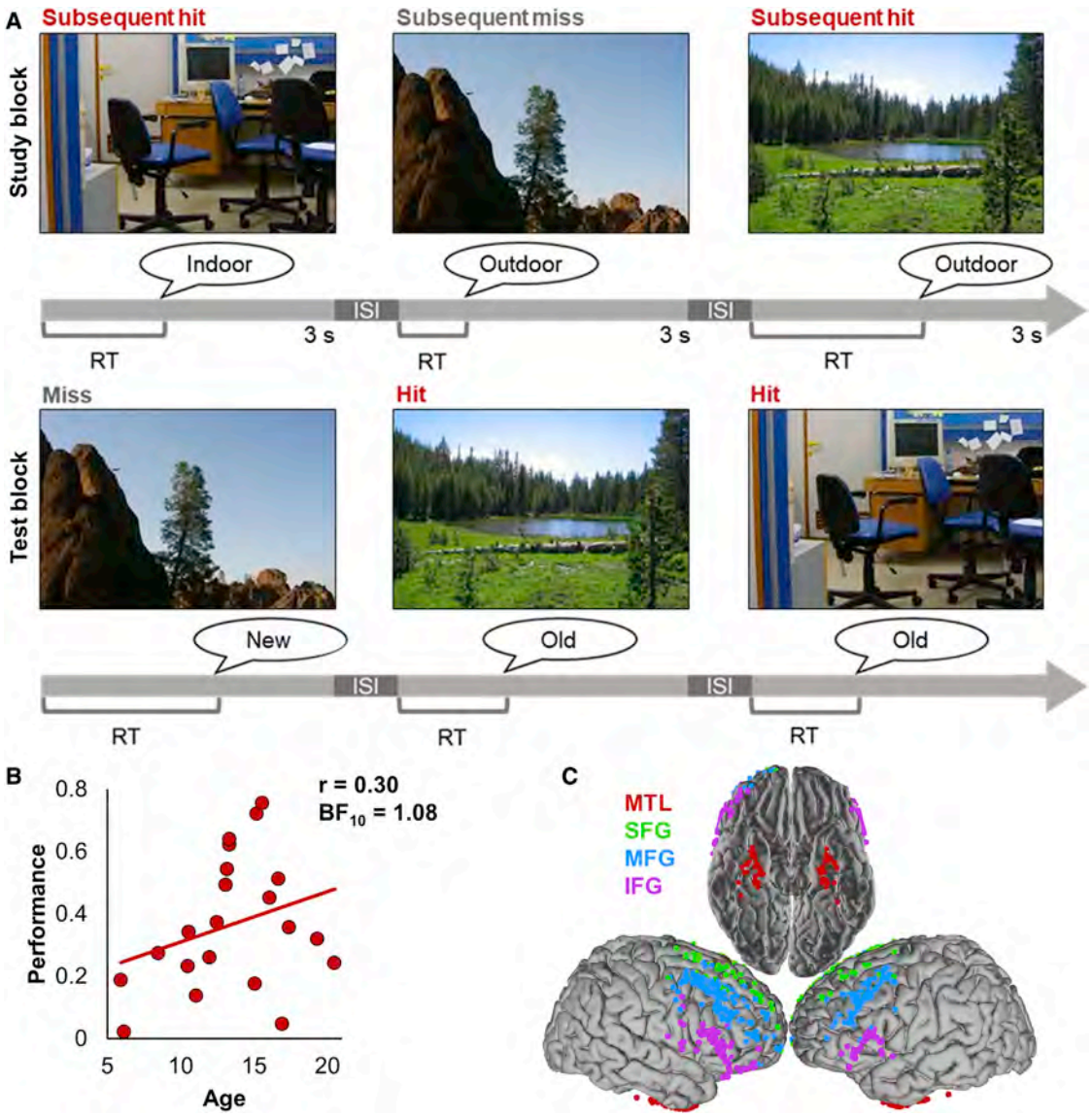

Figure 1. Subsequent memory paradigm, behavior, and electrode coverage

(A) Subsequent memory paradigm. Subjects studied sets of 40 pictures of scenes (3 s each, separated by a 500-ms interstimulus fixation) and made an indoor/outdoor judgment of each scene in preparation for a recognition memory test of all scenes presented during the study block, intermixed with 20 new scenes. Subjects made an old/new judgment of each scene during the test block, which was coded as a hit (red), miss (gray; i.e., new response to a studied scene), correct rejection, or false alarm (old response to new scene). The test was self-paced. ISI, interstimulus interval.

(B) Recognition memory performance generally improved from age 5 to 21 years, with marked inter-individual variability in adolescence. See also Table S1 and Figure S1A.

(C) Reconstruction of artifact-free, nonpathologic electrodes (n = 437) from all subjects. Electrodes are color-coded by region of interest: red, MTL; green, SFG; blue, MFG; purple, IFG. See also Figure S1B.

with typical patterns of MTL theta activity during memory formation in adults.[27] Next, we examined age-related differences in the MTL cluster. Linear mixed-effects modeling indicated non-significant main effects of age ($F(1,17) = 4.22$, $p = 0.056$) and recognition performance ($F(1,17) = 2.78$, $p = 0.114$) and a non-significant interaction ($F(1,17) = 2.26$, $p = 0.151$). No significant clusters were identified using the same analyses to determine spectral signatures of memory formation in PFC (Figure S2), extending our prior examination of high-frequency activity in PFC[42] to the full 1.5–250 Hz spectrum.

Age-related differentiation of the theta band

It has been proposed that decreased power may occur in the presence of narrowband oscillations.[25] Recent studies in adults converge on the finding that two distinct oscillations at the ends of the theta band, centered ~2 and ~8 Hz, support hippocampal processes during memory and navigation.[49–52] Jointly motivated by this literature and the observed spectral signatures of memory formation, we next examined the prevalence of two theta oscillations in cortical sites of the developing brain in a 3-fold procedure. First, visual inspection of study trials (all attended scenes)

Please cite this article in press as: Johnson et al., Dissociable oscillatory theta signatures of memory formation in the developing brain, Current Biology (2022), https://doi.org/10.1016/j.cub.2022.01.053

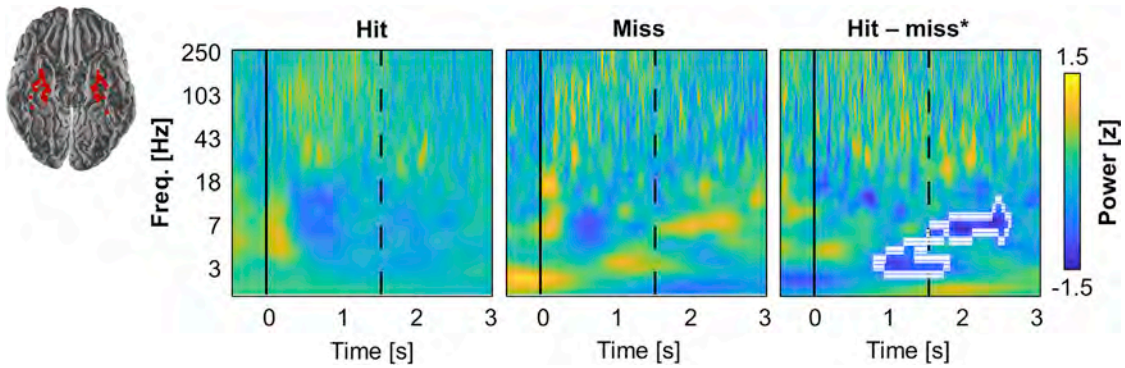

Figure 2. MTL spectral signatures of memory formation

Time-resolved power spectra averaged over all MTL electrodes (n = 80) from all subjects. Left to right: subsequent hit, subsequent miss, cluster-corrected subsequent memory effects. Significant negative subsequent memory effects were identified around the indoor/outdoor response between 2.5 and 10.4 Hz. Stimulus onset is indicated by the vertical line at time = 0 s, and mean RT is indicated by the dashed line. *$p < 0.05$. See also Figure S2.

suggested periodic fluctuations of the ECoG signal in MTL electrodes (Figure 3A, left). Second, a widely utilized irregular sampling procedure separated oscillatory components from the aperiodic 1/f slope.[53] Third, peaks were detected as positive local maxima from the oscillatory components (Figure 3A, right). Across all subjects, we found that most MTL electrodes exhibited periodic fluctuations in the theta band throughout the trial. Fluctuations peaked at both slower (mean ± SD, 2.75 ± 0.47 Hz; 84.4% ± 30.3% electrodes/subject) and faster frequencies (6.81 ± 0.83 Hz; 97.2% ± 8.9% electrodes/subject; Figure 3B).

Analysis of PFC electrodes revealed similar patterns in all regions. In IFG, fluctuations peaked at 2.91 ± 0.51 Hz (89.5% ± 23.3% electrodes/subject) and 7.24 ± 0.65 Hz (99.6% ± 1.7% electrodes/subject; Figure S3). In MFG, fluctuations peaked at 2.91 ± 0.40 Hz (80.1% ± 30.2% electrodes/subject) and 7.07 ± 0.62 Hz (98.7% ± 4.0% electrodes/subject; Figure S4). In SFG, fluctuations peaked at 2.81 ± 0.53 Hz (83.1% ± 24.0% electrodes/subject) and 6.83 ± 0.72 Hz (100% electrodes/subject; Figure S5). These results establish that two theta oscillations are present in cortical sites of the developing MTL and PFC. In addition to extending findings from adults[49–52] to children and adolescents, these results demonstrate that the phenomenon of two theta oscillations is not specific to the hippocampus but extends to frontotemporal networks.

Analysis of age-related differences indicated that the two distinct theta oscillations differentiated in frequency by age in a double dissociation (Figures 3C–3F). Linear mixed-effects modeling revealed a significant interaction of age and frequency in each region (MTL, $F(1,144) = 17.16$, $p = 6 \times 10^{-5}$; IFG, $F(1,192) = 7.28$, $p = 0.008$; MFG, $F(1,358) = 15.96$, $p = 8 \times 10^{-5}$; SFG, $F(1,90) = 6.59$, $p = 0.012$). The 3-way interaction with performance was not significant in any region (MTL, $F(1,140) = 2.24$, $p = 0.137$; IFG, $F(1,188) = 0.03$, $p = 0.856$; MFG, $F(1,354) = 0.08$, $p = 0.772$; SFG, $F(1,86) = 2 \times 10^{-6}$, $p = 0.999$). Thus, in all regions, age was associated with the slowing down of slower oscillations and speeding up of faster oscillations such that, overall, oscillatory peaks were closer to the ends of the canonical theta band in adolescents than in children.

Inter-regional slow theta amplitude coupling signatures of memory formation

Having established that two theta oscillations are prevalent in regions of interest during perception of attended scenes, we addressed our primary aim. We systematically investigated inter-regional interactions between MTL and each PFC region. Specifically, we analyzed theta amplitude coupling independent of phase, theta phase coupling independent of amplitude, and theta phase coupling of high-frequency broadband activity (HFA: 70–150 Hz).[40,54,55] Analyses were performed separately at individually defined slow and fast theta frequencies and excluded electrodes that did not exhibit slow and/or fast theta peaks. Consistent with best practices,[56] this approach ensures that functional connectivity analyses capture oscillatory phenomena of interest[57,58] while controlling for inter-individual differences in these phenomena (Figures 3C–3F).

Inter-regional amplitude coupling was characterized by maximum theta amplitude cross-correlation across serial temporal lags (i.e., amplitude correlation, AC; Figure 4A), indicating both the strength and timing of inter-regional interactions based on oscillatory amplitude.[59] Computations controlled for differences in amplitude between trials and electrodes as they can spuriously drive conditional differences in AC. Cluster-corrected subsequent memory analysis revealed two clusters of higher slow theta AC during the encoding of subsequently recognized relative to forgotten scenes (i.e., positive subsequent memory effects; Figures 4B–4D, top). Effects were identified in IFG-MTL (−0.10 to 0.65 s from scene onset, $p = 0.011$) and MFG-MTL interactions (1.35–1.98 s from scene onset, $p = 0.044$). Neither cluster reflected effects that differed significantly in lag time from zero (Figures 4B–4D, bottom), thus linking memory formation to co-fluctuations of slow theta amplitude as opposed to one region leading the other.[59] The IFG-MTL effect preceded and overlapped with scene onset, consistent with anticipatory processes and exogenous attention, and the MFG-MTL effect overlapped with the mean indoor/outdoor encoding task response, suggestive of semantic decision processes and endogenous attention.[5,60] No significant clusters were identified in fast theta AC (Figures S6A and S6B).

Please cite this article in press as: Johnson et al., Dissociable oscillatory theta signatures of memory formation in the developing brain, Current Biology (2022), https://doi.org/10.1016/j.cub.2022.01.053

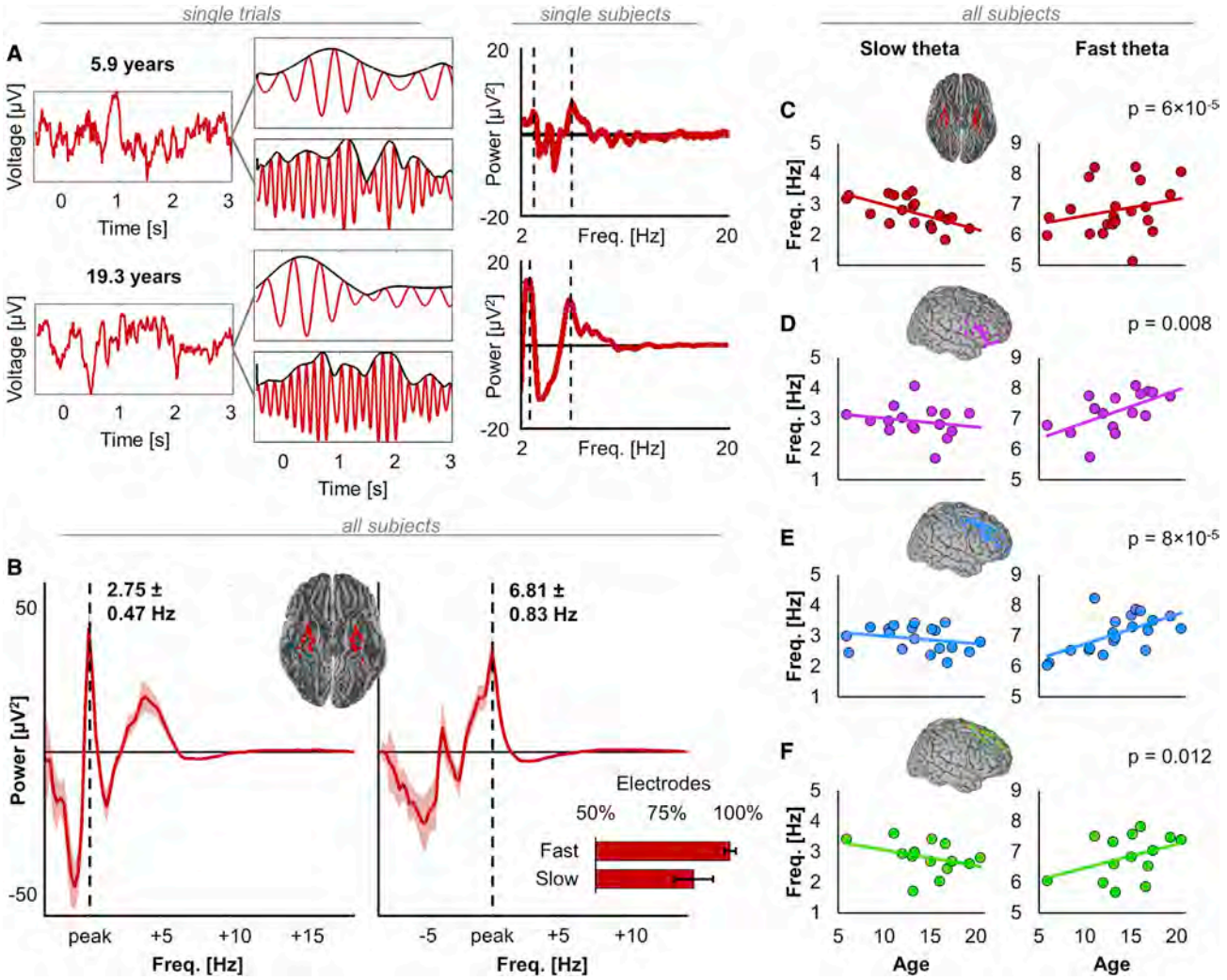

Figure 3. Dual theta oscillations in MTL and age-related differentiation of the theta band

(A) Left: representative single-trial MTL traces, raw and filtered separately at slow and fast theta frequencies, from two subjects aged 5.9 (top) and 19.3 (bottom) years. Black lines are superimposed amplitudes of filtered signals. Right: power spectra from the same electrodes after subtraction of the 1/f slope demonstrate dual theta oscillations in both subjects. See also Figures S3–S5.

(B) Power spectra across all subjects after subtraction of the 1/f slope and peak alignment to individual slow (left) and fast (right) theta frequencies. Inset: slow theta peaks were detected in 84.4% of MTL electrodes/subject and fast theta peaks in 97.2% of electrodes/subject. Shading and error bars indicate SEM across subjects.

(C) MTL dual theta oscillations differentiate in frequency with age in a double dissociation. The p value indicates a significant interaction of frequency (slow versus fast theta) by age.

(D–F) Same as (C) shown separately for IFG (D), MFG (E), and SFG (F).

Inter-regional fast theta phase coupling signatures of memory formation

Inter-regional phase coupling was characterized by maximum theta phase synchrony (i.e., phase-locking value, PLV; Figure 5A, top), indicating the strength of inter-regional interactions based on oscillatory phase.[61] PLV outputs were *Z* score normalized to control for spurious conditional differences, as described in detail in the STAR Methods. Cluster-corrected subsequent memory analysis revealed three clusters of higher fast theta PLV during the encoding of subsequently recognized relative to forgotten scenes (Figures 5B–5D, top). Effects were identified in IFG-MTL interactions (cluster 1, −0.19 to 0.20 s from scene onset, p = 0.01; cluster 2, 2.03–2.43 s from scene onset, p = 0.011) and MFG-MTL interactions (−0.45 to −0.22 s from scene onset, p = 0.05). PLV effects preceded scene onset and followed the mean indoor/outdoor response, again suggesting both anticipatory, exogenous processes and semantic decision, endogenous processes during memory formation.[5,60]

Finally, PFC phase modulation of MTL activity was characterized by maximum cross-frequency synchrony between PFC theta phase and MTL HFA (i.e., phase-amplitude coupling, PAC; Figure 5A, bottom), a mechanism of PFC control over multi-unit neuronal activity in MTL.[40,62,63] PAC computations adopted the PLV approach but replaced the MTL theta signal

Please cite this article in press as: Johnson et al., Dissociable oscillatory theta signatures of memory formation in the developing brain, Current Biology (2022), https://doi.org/10.1016/j.cub.2022.01.053

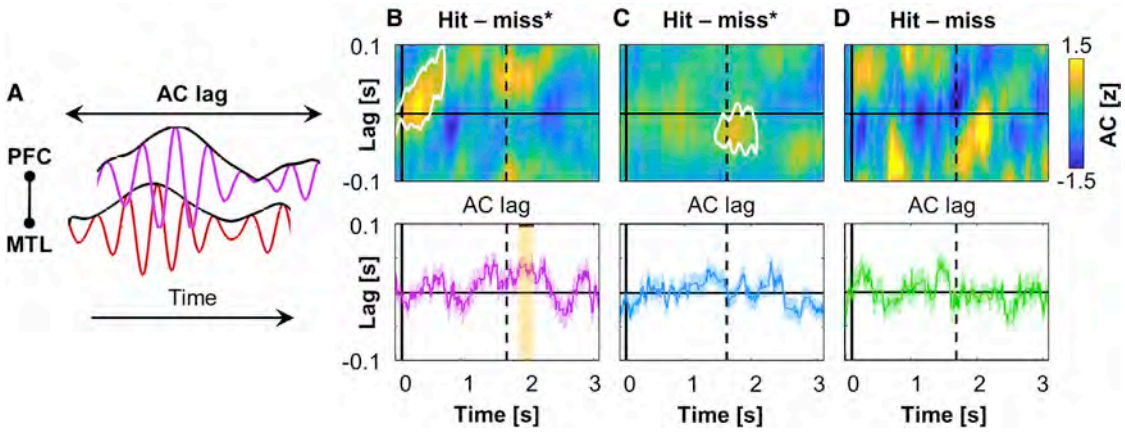

Figure 4. Inter-regional slow theta amplitude coupling signatures of memory formation

(A) AC computation. Amplitudes (black) were extracted from slow theta-filtered signals and AC was computed between pairs of MTL (red) and PFC (IFG shown as an example in magenta) electrodes by correlating the signals over time across serial temporal lags from −0.1 to 0.1 s. Positive lags indicate that PFC leads MTL and negative lags that MTL leads PFC. See also Figures S6A, S6B, and S7.

(B) Cluster-corrected subsequent memory effects in IFG-MTL AC. Top: a significant positive effect was identified around stimulus onset. Bottom: the significant effect did not differ in lag time from zero. A significant lag was identified around the indoor/outdoor response, but it reflected non-significant subsequent memory effects. Stimulus onset is indicated by the vertical line at time = 0 s, and mean RT is indicated by the dashed line. Shading indicates SEM across subjects. Each time point is the midpoint of a 0.5-s epoch (x axis); the first time point of −0.1 s represents −0.35 to 0.15 s from stimulus onset, with the maximum range of −0.45 s pre-stimulus at lag −0.1 s and 0.25 s post-stimulus at lag 0.1 s. *$p < 0.05$.

(C) Same as (B) for MFG-MTL AC. A significant positive subsequent memory effect was identified around the indoor/outdoor response and did not differ significantly in lag time from zero.

(D) Same as (B) for SFG-MTL AC. No significant effects.

with theta-filtered HFA.[64] Cluster-corrected subsequent memory analysis revealed one positive cluster in fast theta MFG-MTL PAC (0.1–0.19 s from scene onset, $p = 0.045$; Figures 5B–5D, bottom). The effect followed scene onset and was brief (<2 fast theta cycles). No significant clusters were identified in slow theta PLV or PAC (Figures S6C and S6D).

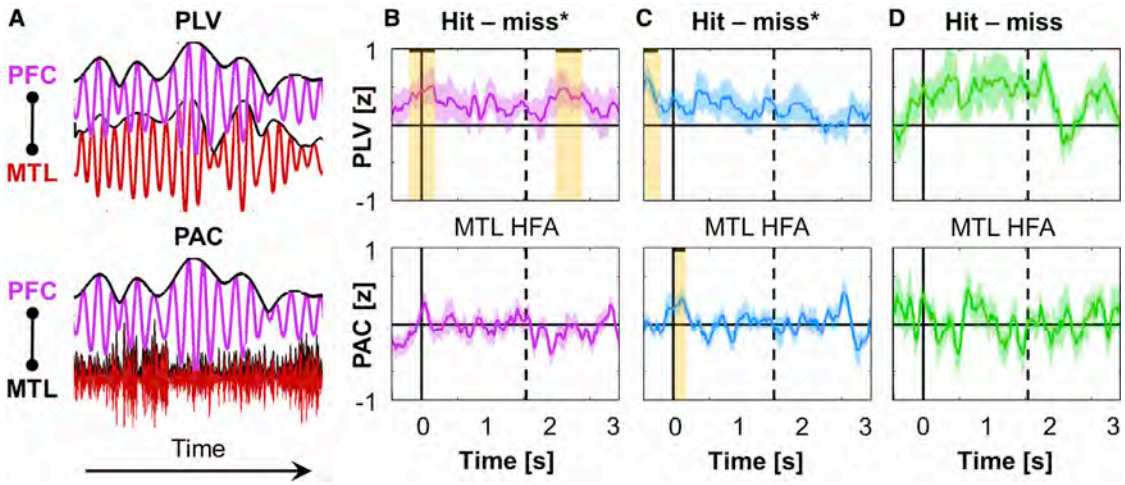

Figure 5. Inter-regional fast theta phase coupling signatures of memory formation

(A) PLV and PAC computation. Top: phases were extracted from fast theta-filtered signals and PLV was computed between pairs of MTL (red) and PFC (IFG shown as an example in magenta) electrodes as time-resolved phase differences. Bottom: phases were extracted from fast theta-filtered signals in PFC and amplitudes (black) were extracted from HFA-filtered signals in MTL. PAC was computed between pairs of MTL and PFC electrodes using the PLV method. See also Figures S6C, S6D, and S7.

(B) Cluster-corrected subsequent memory effects in IFG-MTL PLV and PAC. Top: significant PLV-positive effects were identified around stimulus onset and the indoor/outdoor response. Bottom: no significant PAC effects. Stimulus onset is indicated by the vertical line at time = 0 s, and mean RT is indicated by the dashed line. Shading indicates SEM across subjects. *$p < 0.05$.

(C) Same as (B) for MFG-MTL PLV and PAC. A significant PLV positive subsequent memory effect was identified preceding stimulus onset, and a significant PAC positive effect was identified at stimulus onset.

(D) Same as (B) for SFG-MTL PLV and PAC. No significant effects.

Please cite this article in press as: Johnson et al., Dissociable oscillatory theta signatures of memory formation in the developing brain, Current Biology (2022), https://doi.org/10.1016/j.cub.2022.01.053

Taken together, systematic investigation of interactions between MTL and PFC established that both IFG-MTL and MFG-MTL interactions (1) support memory formation in the developing brain, as posited by theoretical models of memory development;[1–7] (2) reflect dissociable slow theta amplitude and fast theta phase coupling mechanisms;[40,54,55] and (3) occur at distinct epochs. The timing of these interactions suggests anticipatory, exogenous processes, as well as semantic decision, endogenous processes during memory formation.[5,60]

Anticipatory signatures associated with age-related differences in performance

Having characterized dissociable slow and fast theta signatures of inter-regional interactions supporting memory formation in the developing brain, we proceeded to address our second aim. We investigated which of these signatures explain age-related differences in scene recognition performance. Importantly, because functional connectivity analyses controlled for age-related differences in oscillatory theta frequencies (Figures 3C–3F), observation of age-related differences in connectivity signatures would indicate variability specific to coupling strength. As in the analysis of MTL spectral signatures of memory formation, each functional connectivity signature was submitted to a linear mixed-effects model with age and performance as fixed effects. These analyses isolated age-related differences in performance to inter-regional subsequent memory effects preceding scene onset. Specifically, significant interactions of age and performance were identified in slow theta AC between IFG and MTL (Figure 4B, top; $F(1,11) = 9.18$, $p = 0.011$; age, $F(1,11) = 9.75$, $p = 0.010$; performance, $F(1,11) = 8.41$, $p = 0.014$) and in fast theta PLV between MFG and MTL (Figure 5C, top; $F(1,16) = 18.00$, $p = 6 \times 10^{-4}$; age, $F(1,16) = 5.00$, $p = 0.040$; performance, $F(1,16) = 15.20$, $p = 0.001$). In both interactions, top-performing adolescents exhibited the most robust positive subsequent memory effects, relative to both lower-performing adolescents and children (Figure 6).

No other significant interactions of age and performance were identified. This includes the signatures near the mean indoor/outdoor response, slow theta MFG-MTL AC (Figure 4C, top; $F(1,13) = 3.50$, $p = 0.084$; age, $F(1,13) = 1.89$, $p = 0.192$; performance, $F(1,13) = 4.17$, $p = 0.062$) and fast theta IFG-MTL PLV (Figure 5B, top; $F(1,12) = 1.03$, $p = 0.330$; age, $F(1,12) = 0.33$, $p = 0.575$; performance, $F(1,12) = 0.83$, $p = 0.381$). In addition, this includes the fast theta IFG-MTL PLV effect preceding scene onset (Figure 5B, top; $F(1,12) = 1.88$, $p = 0.195$; age, $F(1,12) = 0.76$, $p = 0.400$; performance, $F(1,12) = 1.42$, $p = 0.257$) and the fast theta MFG-MTL PAC effect (Figure 5C, bottom; $F(1,16) = 1.75$, $p = 0.204$; age, $F(1,12) = 1.44$, $p = 0.248$; performance, $F(1,12) = 1.02$, $p = 0.327$).

Collectively, outcomes of these analyses link both slow theta amplitude and fast theta phase coupling mechanisms to age-related differences in scene recognition performance (Figure 6). In both mechanisms, top-performing adolescents exhibited stronger inter-regional oscillatory theta coupling during the encoding of subsequently recognized relative to forgotten scenes, as compared with both lower-performing adolescents and children. The early latency of both effects further suggests that superior performance in adolescents reflects the involvement of anticipatory, exogenous processes in memory formation.

Mapping anticipatory signatures to brain structure

We last sought to identify potential underlying brain structures supporting the slow theta AC and fast theta PLV signatures of scene memory formation that differentiate top-performing adolescents from lower-performing adolescents and children (Figure 6). Specifically, we tested whether distinct inter-regional coupling mechanisms in top-performing adolescents were more likely to reflect the maturation of the same white matter tract or distinct tracts. We focused *a priori* on the cingulum and uncinate, as they are the major tracts connecting MTL and PFC.[10,11] These tracts are thus candidate brain structures supporting age-related differences in episodic memory.[2]

Diffusion-weighted imaging (DWI) data were available for 11 of the 21 subjects in the sample, aged 6.2–16.7 years (Table S1). We performed function-structure mapping of oscillatory theta subsequent memory effects and paired DWI of the cingulum and uncinate in a 2-fold procedure. First, the structural integrity of each tract, indexed by tractography-weighted fractional anisotropy (FA), was submitted to a linear mixed-effects model with age and performance as fixed effects. Outcomes link age-related differences in scene recognition performance to the cingulum by means of a significant interaction ($F(1,7) = 5.68$, $p = 0.049$; age, $F(1,7) = 1.25$, $p = 0.300$, performance, $F(1,7) = 3.47$, $p = 0.105$; Figure 7A). Top-performing adolescents exhibited higher FA in the cingulum than lower-performing adolescents and children. Modeling of the uncinate indicated a non-significant interaction ($F(1,7) = 1.03$, $p = 0.344$, age, $F(1,7) = 0.44$, $p = 0.529$, performance, $F(1,7) = 0.67$, $p = 0.804$; Figure 7B). Indeed, analysis of main effects only, excluding the interaction term, identified a significant effect of performance ($F(1,8) = 9.62$, $p = 0.015$) that was not related to age ($F(1,8) = 0.01$, $p = 0.928$). These results are consistent with existing literature in large non-clinical cohorts[65] and suggest that age-related differences in inter-regional functional coupling measures are likely to reflect maturation of the cingulum, where a comparable interaction of age and performance was identified.

Second, Bayesian correlation tested the specific hypothesis that the slow theta AC and fast theta PLV signatures, which differentiate top-performing adolescents from lower-performing adolescents and children, were likely to reflect maturation of the cingulum. Consistent with this hypothesis, cingulum FA was positively correlated with both the slow theta IFG-MTL AC ($r = 0.50$, 95% CI 0.03–0.84, $BF_{10} = 1.48$) and fast theta MFG-MTL PLV ($r = 0.64$, 95% CI 0.08–0.87, $BF_{10} = 4.31$; Figure 7C) effects. Uncinate FA, in contrast, was unlikely to correlate with either effect ($BF_{10} \leq 0.81$; Figure 7D). Age-related differences in slow theta AC and fast theta PLV signatures of memory formation likely reflect maturation of the cingulum. These results suggest that age-related differences in multiplexing, wherein the same structural tract concurrently supports dissociable functional signatures of memory formation,[22] differentiate top-performing adolescents from lower-performing adolescents and children.

DISCUSSION

Understanding complex human brain functions is critically informed by studying such functions during development. Here, we used a rare opportunity to examine the functional neurophysiology and structural anatomy of episodic memory

Please cite this article in press as: Johnson et al., Dissociable oscillatory theta signatures of memory formation in the developing brain, Current Biology (2022), https://doi.org/10.1016/j.cub.2022.01.053

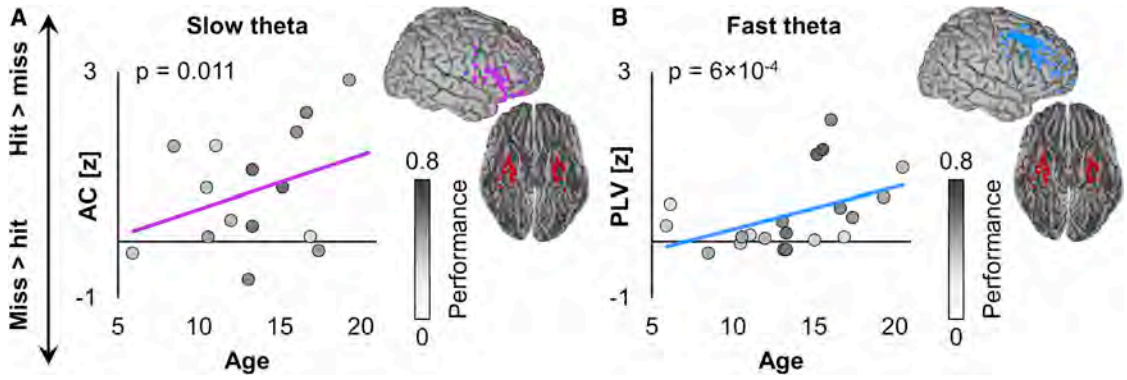

Figure 6. Inter-regional signatures associated with age-related differences in performance

(A) The slow theta IFG-MTL AC signature of memory formation around stimulus onset explains age-related differences in recognition performance (Figure 4B, top).

(B) The fast theta MFG-MTL PLV signature of memory formation preceding stimulus onset explains age-related differences in recognition performance (Figure 5C, top).

formation in children and adolescents undergoing subdural monitoring of MTL and PFC.[6,22] Our data demonstrate that neural oscillations in the theta band provide the functional infrastructure for MTL-PFC interactions during memory formation in the human brain. MTL and PFC interact via dissociable theta mechanisms during memory formation, an ~3-Hz oscillation that supports inter-regional amplitude coupling and slows down with age, and an ~7-Hz oscillation that supports inter-regional phase coupling and speeds up with age. These findings establish neurophysiological signatures of memory formation in children and adolescents. Amplitude and phase coupling signatures preceding stimulus onset further differentiated top-performing adolescents from lower-performing adolescents and children, suggesting that age-related differences in anticipatory, exogenous attention contribute to memory development. Both memory-related theta signatures likely reflect maturation of the cingulum. Based on these findings, we propose that the development of multiplexed oscillatory interactions, wherein the same structural

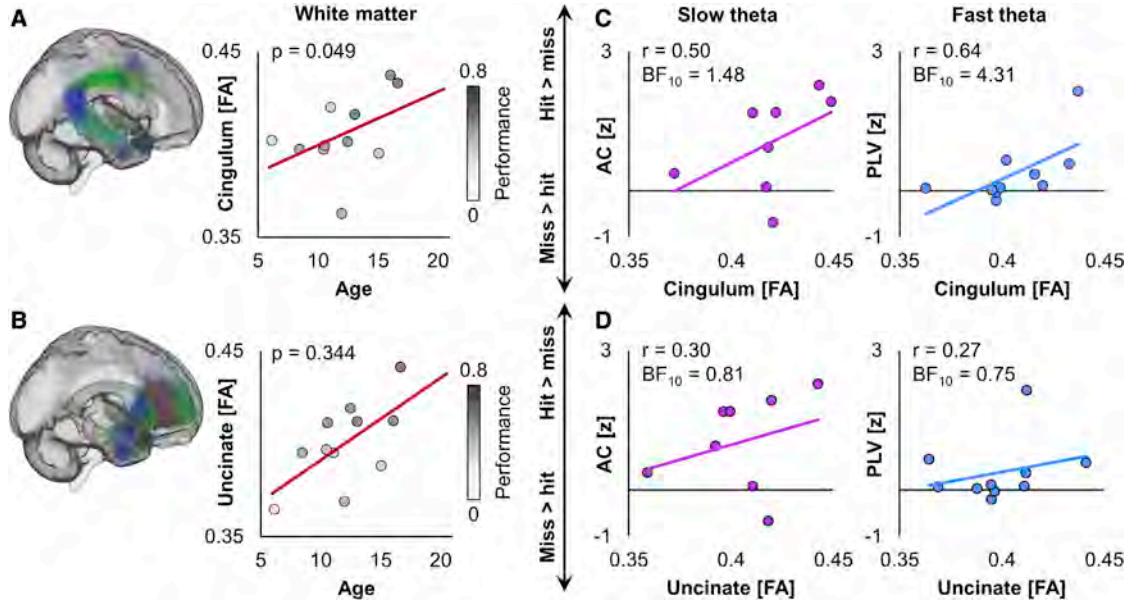

Figure 7. Structural tracts associated with age-related differences in performance

(A) Left: cingulum tracts across subjects (n = 11). Right: cingulum integrity explains age-related differences in recognition performance. The p value indicates a significant interaction of age and performance.

(B) Same as (A) for the uncinate tract. Non-significant interaction of age and performance.

(C) Cingulum integrity is positively correlated with both the slow theta IFG-MTL AC (left) and fast theta MFG-MTL PLV (right) signatures of memory formation, which explain age-related differences in recognition performance (Figure 6).

(D) Same as (C) for the uncinate tract. Uncinate integrity is not correlated with either signature.

Please cite this article in press as: Johnson et al., Dissociable oscillatory theta signatures of memory formation in the developing brain, Current Biology (2022), https://doi.org/10.1016/j.cub.2022.01.053

tract (i.e., cingulum) supports dissociable functional mechanisms (slow theta amplitude coupling, fast theta phase coupling), underlies the development of episodic memory. Our findings point to a novel mechanistic explanation of how MTL-PFC interactions support memory formation in children and adolescents, addressing a major outstanding question in theoretical models of memory.[1–7]

Importantly, before testing specific hypotheses, we demonstrated that our pediatric patient sample represents typical memory development. First, behavioral performance on the established scene recognition memory task we used correlated positively with age, with marked inter-individual variability among adolescents. This result replicates reports from non-clinical cohorts[6,14,18,44,45] and motivated identification of signatures of memory formation that differentiate top-performing adolescents from both lower-performing adolescents and children. Second, analysis of MTL power during the perception of subsequently recognized compared to forgotten scenes revealed decreased activity at theta frequencies during successful memory formation. These theta signatures of memory formation are consistent with patterns typically observed in adults.[27] It is possible that decreased power in the presence of narrowband oscillations enables long-range connectivity, manifesting as decreased power within a region (here, MTL) and increased connectivity between regions.[25] Accordingly, further analyses focused on narrowband oscillations and MTL-PFC connectivity.

Based on our finding of power subsequent memory effects across lower and higher theta frequency ranges, and motivated by burgeoning reports in adults,[49–52] we next tested for the presence of two theta oscillations in our pediatric sample. Results establish two theta oscillations in cortical sites of the developing MTL and PFC, thus extending the phenomenon from adults to children and adolescents, and from the hippocampus to frontotemporal networks. Further analyses uncovered the remarkable finding that age was associated with the speeding of oscillations ~7 Hz and slowing of oscillations ~3 Hz in all regions, such that frequencies only approached the ends of the canonical theta band in adolescents. These outcomes suggest that theta oscillations differentiate in a double dissociation over a protracted developmental trajectory.

Since the first human electroencephalogram (EEG) studies, developmental research has focused on the scalp-dominant alpha band, defined by a frequency of 8–12 Hz in adults. Alpha oscillations appear at 3–4 Hz during infancy, speed up to 5–7 Hz during the first year of life, and reach adult-level frequencies around 12 years of age.[66–68] These data summarize longitudinal studies published between 1939 and 2020. Building on this foundational literature, we previously showed that attention-related alpha oscillations in primary visual cortex speed up with age during performance of the same task.[43] Here, we reveal that development is not only associated with the speeding of oscillations but also differentiation of the memory-relevant theta band to adult levels. Whereas faster oscillations reflect faster fluctuations between neuronal excitation and inhibition,[37] potentially subserving increased information processing during visual attention,[43] slower oscillations reflect more prolonged periods of excitation, potentially subserving increased information integration.[38] However, although age differences in theta frequencies were robust throughout the frontotemporal network, they did not explain scene recognition performance. Our findings thus raise the intriguing possibility that differentiation of the theta band is a core aspect of brain development, which may be pervasive across both brain regions and task contexts.

Systematic investigation of normalized MTL-PFC interactions at slow and fast theta, after controlling for inter-individual differences, determined signatures of memory formation. Both slow theta amplitude and fast theta phase coupling supported MTL-PFC interactions predictive of memory formation. Significant subsequent memory effects were observed in interactions between MTL and IFG and MFG at epochs immediately preceding scene onset, likely related to anticipatory, exogenous processes, and near the mean indoor/outdoor encoding task response, suggesting semantic decision, endogenous processes.[5,60] In addition, fast theta MFG-MTL PAC, a mechanism of prefrontal control over MTL,[40] was greater immediately following the onset of subsequently recognized compared to forgotten scenes. We did not find any significant overlap in coupling mechanisms across slow and fast theta frequencies. Whereas the oscillatory phase relationship between regions is theorized to dictate the strength of communication,[41] co-fluctuations of amplitude provide a putative mechanism for intra-regional functions to co-occur.[54] Fast theta phase coupling may thus serve as a signature of memory formation, which reflects inter-regional communication, and co-fluctuations of slow theta amplitude provide a complementary signature that is dissociable in both frequency and mechanism.[40,54,55] These slow and fast theta signatures become increasingly dissociable in frequency across development.

Some, but not all, MTL-PFC signatures of memory formation further differentiated top-performing adolescents from not only children but also lower-performing adolescents.[6,42,43] Only signatures that preceded stimulus onset significantly explained age-related differences in recognition performance. Notably, these signatures included both coupling mechanisms, slow theta amplitude coupling between MTL and IFG and fast theta phase coupling between MTL and MFG. The timing of both effects suggests that superior performance in adolescents reflects anticipatory, exogenous processes involved in memory formation, and these processes are supported by dissociable mechanisms of interaction between MTL and PFC.

Finally, whereas the concurrence of effects may imply multiplexed interactions, the divergence in mechanism and PFC region by effect paradoxically implies either multiplexing or distinct interactions along distinct pathways. Indeed, structure-function relationships in brain connectivity are notoriously complex.[69,70] To disentangle these alternatives, we analyzed paired diffusion data of the cingulum and uncinate tracts from a subset of patients. Bayesian analysis provided an initial test due to limitations of the small sample[71] and suggested that age-related differences in both coupling mechanisms reflect maturation of the cingulum. Given that cingulum integrity also differentiated top-performing adolescents from both lower-performing adolescents and children, we propose that the development of multiplexed theta interactions underlies memory development. We further speculate that development of any cognitive function that relies on anticipatory, exogenous attention is driven in part by development of the same neurophysiological phenomena.

Please cite this article in press as: Johnson et al., Dissociable oscillatory theta signatures of memory formation in the developing brain, Current Biology (2022), https://doi.org/10.1016/j.cub.2022.01.053

Limitations

This study is limited by the sample size. Intracranial studies are often based on few patients with effects replicated per patient. Such an approach is qualified by the high signal quality of the data, which enables single-trial precision and single-subject reliability.[27,72] However, because we aimed to identify inter-individual differences across development, our study required group-level analysis of single-subject data.[6] Group-level analysis necessitated defining regions of interest based on a sufficiently large anatomical space to encompass inter-individual variability in coverage (e.g., entire cortical gyri).[42,43] Lost with this approach was the potential to detect meaningful variability in effects within a region, although future studies may address this limitation by increasing the sample size. The sample of 21 subjects achieves 80% power to detect large effects and is likely to miss smaller effects (i.e., type II error).[73] To disentangle smaller, sub-threshold effects from null effects, we used Bayesian analysis[71] and validated estimates by comparison against extant literature in large non-clinical samples. We caution against over-interpreting (1) non-significant effects, especially in subsets of the sample (e.g., SFG effects[42]); and (2) diffusion tractography results, which provide initial evidence of multiplexing based on half of the sample. Pediatric intracranial research is a burgeoning field that relies on the availability of neurosurgical patients who fit study criteria. As the field grows, future research may seek to increase sample sizes through multi-site collaboration and data sharing.[6]

Conclusions

We addressed a major gap in models of human memory by leveraging a rare opportunity to investigate the neurophysiological mechanisms of MTL-PFC interactions supporting memory formation in the developing brain. We confirm the importance of theta oscillations to episodic memory and demonstrate a remarkable dissociation of slow and fast theta frequencies across development. This finding raises fundamental questions about the development of frontotemporal networks and cognition broadly. In addressing our primary goal of identifying the mechanisms of MTL-PFC interactions, we establish a functional dissociation between slow theta amplitude coupling and fast theta phase coupling signatures of memory formation. Second, we found that slow and fast theta interactions immediately preceding scene onset further explained age-related differences in recognition performance, suggesting that age effects are tied to general attentional control. Lastly, we provide initial evidence that distinct age-related signatures of MTL-PFC interactions are linked to age-related differences in the integrity of the cingulum tract, suggesting age-related differences in multiplexing. Collectively, our findings establish system-level dynamics of memory formation, critically extend models of memory development based on noninvasive neuroimaging, and illuminate dissociable frontotemporal networks during attentional control as core mechanisms in models of memory development.

STAR★METHODS

Detailed methods are provided in the online version of this paper and include the following:

- KEY RESOURCES TABLE
- RESOURCE AVAILABILITY
  - Lead contact
  - Materials availability
  - Data and code availability
- EXPERIMENTAL MODEL AND SUBJECT DETAILS
  - Human subjects
- METHOD DETAILS
  - Memory task
  - Electrocorticography
  - Structural imaging
- QUANTIFICATION AND STATISTICAL ANALYSIS
  - Behavior
  - Spectral decomposition
  - Oscillatory peak detection
  - Inter-regional amplitude coupling
  - Inter-regional phase coupling
  - Inter-regional phase-amplitude coupling
  - Exploratory inter-regional analyses
  - Subsequent memory
  - Inter-individual differences

SUPPLEMENTAL INFORMATION

Supplemental information can be found online at https://doi.org/10.1016/j.cub.2022.01.053.

ACKNOWLEDGMENTS

We thank K.L. Canada, R.T. Knight, and J.J. Lin for support, and N. Kuroda, M. Sonoda, M. Malik, C. Miller Rigoli, R.F. Schwarzlose, X. Chen, and A.T. Shafer for assistance. This work was funded by grants from the National Institutes of Health (NIMH R01MH107512, NINDS R00NS115918, NINDS R01NS64033, and NINDS R01089659).

AUTHOR CONTRIBUTIONS

Conceptualization, E.L.J., N.O., and Q.Y.; data curation, E.L.J., Q.Y., N.B.O., and L.T.; formal analysis, E.L.J. and N.B.O.; funding acquisition, N.O., E.L.J., J.-W.J., and E.A.; investigation, E.A. and N.O.; methodology, N.O.; software, E.L.J., Q.Y., N.B.O., and L.T.; supervision, N.O., J.-W.J., and E.A.; validation, E.L.J., N.B.O., J.-W.J., and N.O.; visualization, E.L.J., Q.Y., N.B.O., L.T., and N.O.; writing – original draft, E.L.J., N.B.O., and N.O.; writing – review & editing, E.L.J., N.O., Q.Y., N.B.O., J.-W.J., and E.A.

DECLARATION OF INTERESTS

The authors declare no competing interests.

Received: October 27, 2021
Revised: December 15, 2021
Accepted: January 19, 2022
Published: February 15, 2022

REFERENCES

1. Werkle-Bergner, M., Müller, V., Li, S.C., and Lindenberger, U. (2006). Cortical EEG correlates of successful memory encoding: implications for lifespan comparisons. Neurosci. Biobehav. Rev. *30*, 839–854.
2. Ghetti, S., and Bunge, S.A. (2012). Neural changes underlying the development of episodic memory during middle childhood. Dev. Cogn. Neurosci. *2*, 381–395.
3. Ofen, N. (2012). The development of neural correlates for memory formation. Neurosci. Biobehav. Rev. *36*, 1708–1717.

Please cite this article in press as: Johnson et al., Dissociable oscillatory theta signatures of memory formation in the developing brain, Current Biology (2022), https://doi.org/10.1016/j.cub.2022.01.053

4. Ofen, N., and Shing, Y.L. (2013). From perception to memory: changes in memory systems across the lifespan. Neurosci. Biobehav. Rev. *37*, 2258–2267.
5. Ofen, N., Yu, Q., and Chen, Z. (2016). Memory and the developing brain: are insights from cognitive neuroscience applicable to education? Curr. Opin. Behav. Sci. *10*, 81–88.
6. Ofen, N., Tang, L., Yu, Q., and Johnson, E.L. (2019). Memory and the developing brain: from description to explanation with innovation in methods. Dev. Cogn. Neurosci. *36*, 100613.
7. Keresztes, A., Ngo, C.T., Lindenberger, U., Werkle-Bergner, M., and Newcombe, N.S. (2018). Hippocampal maturation drives memory from generalization to specificity. Trends Cogn. Sci. *22*, 676–686.
8. Sowell, E.R., Thompson, P.M., Leonard, C.M., Welcome, S.E., Kan, E., and Toga, A.W. (2004). Longitudinal mapping of cortical thickness and brain growth in normal children. J. Neurosci. *24*, 8223–8231.
9. Gogtay, N., Giedd, J.N., Lusk, L., Hayashi, K.M., Greenstein, D., Vaituzis, A.C., Nugent, T.F., Herman, D.H., Clasen, L.S., Toga, A.W., and Rapoport, J.L. (2004). Dynamic mapping of human cortical development during childhood through early adulthood. Proc. Natl. Acad. Sci. USA *101*, 8174–8179.
10. Lebel, C., and Beaulieu, C. (2011). Longitudinal development of human brain wiring continues from childhood into adulthood. J. Neurosci. *31*, 10937–10947.
11. Lebel, C., Gee, M., Camicioli, R., Wieler, M., Martin, W., and Beaulieu, C. (2012). Diffusion tensor imaging of white matter tract evolution over the lifespan. Neuroimage *60*, 340–352.
12. Sydnor, V.J., Larsen, B., Bassett, D.S., Alexander-Bloch, A., Fair, D.A., Liston, C., Mackey, A.P., Milham, M.P., Pines, A., Roalf, D.R., et al. (2021). Neurodevelopment of the association cortices: patterns, mechanisms, and implications for psychopathology. Neuron *109*, 2820–2846.
13. Menon, V., Boyett-Anderson, J.M., and Reiss, A.L. (2005). Maturation of medial temporal lobe response and connectivity during memory encoding. Brain Res. Cogn. Brain Res. *25*, 379–385.
14. Ofen, N., Kao, Y.-C., Sokol-Hessner, P., Kim, H., Whitfield-Gabrieli, S., and Gabrieli, J.D.E. (2007). Development of the declarative memory system in the human brain. Nat. Neurosci. *10*, 1198–1205.
15. Shing, Y.L., Werkle-Bergner, M., Brehmer, Y., Müller, V., Li, S.C., and Lindenberger, U. (2010). Episodic memory across the lifespan: the contributions of associative and strategic components. Neurosci. Biobehav. Rev. *34*, 1080–1091.
16. Sander, M.C., Werkle-Bergner, M., Gerjets, P., Shing, Y.L., and Lindenberger, U. (2012). The two-component model of memory development, and its potential implications for educational settings. Dev. Cogn. Neurosci. *2* (*Suppl 1*), S67–S77.
17. Müller, N.C.J., Kohn, N., van Buuren, M., Klijn, N., Emmen, H., Berkers, R.M.W.J., Dresler, M., Janzen, G., and Fernández, G. (2021). Differences in executive abilities rather than associative processes contribute to memory development. Hum. Brain Mapp. *42*, 6000–6013.
18. Tang, L., Shafer, A.T., and Ofen, N. (2018). Prefrontal cortex contributions to the development of memory formation. Cereb. Cortex *28*, 3295–3308.
19. Shing, Y.L., Brehmer, Y., Heekeren, H.R., Bäckman, L., and Lindenberger, U. (2016). Neural activation patterns of successful episodic encoding: reorganization during childhood, maintenance in old age. Dev. Cogn. Neurosci. *20*, 59–69.
20. Geng, F., Redcay, E., and Riggins, T. (2019). The influence of age and performance on hippocampal function and the encoding of contextual information in early childhood. Neuroimage *195*, 433–443.
21. Qin, S., Cho, S., Chen, T., Rosenberg-Lee, M., Geary, D.C., and Menon, V. (2014). Hippocampal-neocortical functional reorganization underlies children's cognitive development. Nat. Neurosci. *17*, 1263–1269.
22. Johnson, E.L., and Knight, R.T. (2015). Intracranial recordings and human memory. Curr. Opin. Neurobiol. *31*, 18–25.
23. Matsumoto, J.Y., Stead, M., Kucewicz, M.T., Matsumoto, A.J., Peters, P.A., Brinkmann, B.H., Danstrom, J.C., Goerss, S.J., Marsh, W.R., Meyer, F.B., and Worrell, G.A. (2013). Network oscillations modulate interictal epileptiform spike rate during human memory. Brain *136*, 2444–2456.
24. Lin, J.-J., Rugg, M.D., Das, S., Stein, J., Rizzuto, D.S., Kahana, M.J., and Lega, B.C. (2017). Theta band power increases in the posterior hippocampus predict successful episodic memory encoding in humans. Hippocampus *27*, 1040–1053.
25. Herweg, N.A., Solomon, E.A., and Kahana, M.J. (2020). Theta oscillations in human memory. Trends Cogn. Sci. *24*, 208–227.
26. Serruya, M.D., Sederberg, P.B., and Kahana, M.J. (2014). Power shifts track serial position and modulate encoding in human episodic memory. Cereb. Cortex *24*, 403–413.
27. Johnson, E.L., Kam, J.W.Y., Tzovara, A., and Knight, R.T. (2020). Insights into human cognition from intracranial EEG: a review of audition, memory, internal cognition, and causality. J. Neural Eng. *17*, 051001.
28. Shin, J.D., and Jadhav, S.P. (2016). Multiple modes of hippocampal–prefrontal interactions in memory-guided behavior. Curr. Opin. Neurobiol. *40*, 161–169.
29. Long, N.M., Burke, J.F., and Kahana, M.J. (2014). Subsequent memory effect in intracranial and scalp EEG. Neuroimage *84*, 488–494.
30. Long, N.M., and Kahana, M.J. (2015). Successful memory formation is driven by contextual encoding in the core memory network. Neuroimage *119*, 332–337.
31. Greenberg, J.A., Burke, J.F., Haque, R., Kahana, M.J., and Zaghloul, K.A. (2015). Decreases in theta and increases in high frequency activity underlie associative memory encoding. Neuroimage *114*, 257–263.
32. Kragel, J.E., Ezzyat, Y., Sperling, M.R., Gorniak, R., Worrell, G.A., Berry, B.M., Inman, C., Lin, J.-J., Davis, K.A., Das, S.R., et al. (2017). Similar patterns of neural activity predict memory function during encoding and retrieval. Neuroimage *155*, 60–71.
33. Burke, J.F., Zaghloul, K.A., Jacobs, J., Williams, R.B., Sperling, M.R., Sharan, A.D., and Kahana, M.J. (2013). Synchronous and asynchronous theta and gamma activity during episodic memory formation. J. Neurosci. *33*, 292–304.
34. Solomon, E.A., Kragel, J.E., Sperling, M.R., Sharan, A., Worrell, G., Kucewicz, M., Inman, C.S., Lega, B., Davis, K.A., Stein, J.M., et al. (2017). Widespread theta synchrony and high-frequency desynchronization underlies enhanced cognition. Nat. Commun. *8*, 1704.
35. Gruber, M.J., Hsieh, L.-T., Staresina, B.P., Elger, C.E., Fell, J., Axmacher, N., and Ranganath, C. (2018). Theta phase synchronization between the human hippocampus and prefrontal cortex increases during encoding of unexpected information: a case study. J. Cogn. Neurosci. *30*, 1646–1656.
36. Lega, B.C., Jacobs, J., and Kahana, M. (2012). Human hippocampal theta oscillations and the formation of episodic memories. Hippocampus *22*, 748–761.
37. Buzsáki, G., and Draguhn, A. (2004). Neuronal oscillations in cortical networks. Science *304*, 1926–1929.
38. Buzsáki, G. (2002). Theta oscillations in the hippocampus. Neuron *33*, 325–340.
39. Nyhus, E., and Curran, T. (2010). Functional role of gamma and theta oscillations in episodic memory. Neurosci. Biobehav. Rev. *34*, 1023–1035.
40. Helfrich, R.F., and Knight, R.T. (2016). Oscillatory dynamics of prefrontal cognitive control. Trends Cogn. Sci. *20*, 916–930.
41. Fries, P. (2005). A mechanism for cognitive dynamics: neuronal communication through neuronal coherence. Trends Cogn. Sci. *9*, 474–480.
42. Johnson, E.L., Tang, L., Yin, Q., Asano, E., and Ofen, N. (2018). Direct brain recordings reveal prefrontal cortex dynamics of memory development. Sci. Adv. *4*, eaat3702.
43. Yin, Q., Johnson, E.L., Tang, L., Auguste, K.I., Knight, R.T., Asano, E., and Ofen, N. (2020). Direct brain recordings reveal occipital cortex involvement in memory development. Neuropsychologia *148*, 107625.
44. Chai, X.J., Ofen, N., Gabrieli, J.D.E., and Whitfield-Gabrieli, S. (2014). Development of deactivation of the default-mode network during episodic memory formation. Neuroimage *84*, 932–938.

Please cite this article in press as: Johnson et al., Dissociable oscillatory theta signatures of memory formation in the developing brain, Current Biology (2022), https://doi.org/10.1016/j.cub.2022.01.053

45. Chai, X.J., Ofen, N., Jacobs, L.F., and Gabrieli, J.D. (2010). Scene complexity: influence on perception, memory, and development in the medial temporal lobe. Front. Hum. Neurosci. *4*, 21.

46. Tang, L., Pruitt, P.J., Yu, Q., Homayouni, R., Daugherty, A.M., Damoiseaux, J.S., and Ofen, N. (2020). Differential functional connectivity in anterior and posterior hippocampus supporting the development of memory formation. Front. Hum. Neurosci. *14*, 204.

47. Tang, L., Yu, Q., Homayouni, R., Canada, K.L., Yin, Q., Damoiseaux, J.S., and Ofen, N. (2021). Reliability of subsequent memory effects in children and adults: the good, the bad, and the hopeful. Dev. Cogn. Neurosci. *52*, 101037.

48. Maris, E., and Oostenveld, R. (2007). Nonparametric statistical testing of EEG- and MEG-data. J. Neurosci. Methods *164*, 177–190.

49. Goyal, A., Miller, J., Qasim, S.E., Watrous, A.J., Zhang, H., Stein, J.M., Inman, C.S., Gross, R.E., Willie, J.T., Lega, B., et al. (2020). Functionally distinct high and low theta oscillations in the human hippocampus. Nat. Commun. *11*, 2469.

50. Choi, K., Bagen, L., Robinson, L., Umbach, G., Rugg, M., and Lega, B. (2020). Longitudinal differences in human hippocampal connectivity during episodic memory processing. Cereb. Cortex Commun. *1*, tgaa010.

51. Vivekananda, U., Bush, D., Bisby, J.A., Baxendale, S., Rodionov, R., Diehl, B., Chowdhury, F.A., McEvoy, A.W., Miserocchi, A., Walker, M.C., et al. (2021). Theta power and theta-gamma coupling support spatial memory retrieval. Hippocampus *31*, 213–220.

52. Kota, S., Rugg, M.D., and Lega, B.C. (2020). Hippocampal theta oscillations support successful associative memory formation. J. Neurosci. *40*, 9507–9518.

53. Wen, H., and Liu, Z. (2016). Separating fractal and oscillatory components in the power spectrum of neurophysiological signal. Brain Topogr. *29*, 13–26.

54. Mostame, P., and Sadaghiani, S. (2020). Phase- and amplitude-coupling are tied by an intrinsic spatial organization but show divergent stimulus-related changes. Neuroimage *219*, 117051.

55. Siems, M., and Siegel, M. (2020). Dissociated neuronal phase- and amplitude-coupling patterns in the human brain. Neuroimage *209*, 116538.

56. Donoghue, T., Schaworonkow, N., and Voytek, B. (2021). Methodological considerations for studying neural oscillations. Eur. J. Neurosci. Published online July 16, 2021. https://doi.org/10.1111/ejn.15361.

57. Stolk, A., Brinkman, L., Vansteensel, M.J., Aarnoutse, E., Leijten, F.S.S., Dijkerman, C.H., Knight, R.T., Lange, F.P. de, and Toni, I. (2019). Electrocorticographic dissociation of alpha and beta rhythmic activity in the human sensorimotor system. eLife *8*, e48065.

58. Donoghue, T., Haller, M., Peterson, E.J., Varma, P., Sebastian, P., Gao, R., Noto, T., Lara, A.H., Wallis, J.D., Knight, R.T., et al. (2020). Parameterizing neural power spectra into periodic and aperiodic components. Nat. Neurosci. *23*, 1655–1665.

59. Adhikari, A., Sigurdsson, T., Topiwala, M.A., and Gordon, J.A. (2010). Cross-correlation of instantaneous amplitudes of field potential oscillations: a straightforward method to estimate the directionality and lag between brain areas. J. Neurosci. Methods *191*, 191–200.

60. Johnson, E.L., Munro, S.E., and Bunge, S.A. (2014). Development of neural networks supporting goal-directed behavior. In Minnesota Symposia on Child Psychology: Developing Cognitive Control Processes: Mechanisms, Implications, and Interventions, P.D. Zelazo, and M. Sera, eds. (John Wiley & Sons, Inc.).

61. Lachaux, J.P., Rodriguez, E., Martinerie, J., and Varela, F.J. (1999). Measuring phase synchrony in brain signals. Hum. Brain Mapp. *8*, 194–208.

62. Voytek, B., Kayser, A.S., Badre, D., Fegen, D., Chang, E.F., Crone, N.E., Parvizi, J., Knight, R.T., and D'Esposito, M. (2015). Oscillatory dynamics coordinating human frontal networks in support of goal maintenance. Nat. Neurosci. *18*, 1318–1324.

63. Friese, U., Köster, M., Hassler, U., Martens, U., Trujillo-Barreto, N., and Gruber, T. (2013). Successful memory encoding is associated with increased cross-frequency coupling between frontal theta and posterior gamma oscillations in human scalp-recorded EEG. Neuroimage *66*, 642–647.

64. Penny, W.D., Duzel, E., Miller, K.J., and Ojemann, J.G. (2008). Testing for nested oscillation. J. Neurosci. Methods *174*, 50–61.

65. Wendelken, C., Lee, J.K., Pospisil, J., Sastre, M., Ross, J.M., Bunge, S.A., and Ghetti, S. (2015). White matter tracts connected to the medial temporal lobe support the development of mnemonic control. Cereb. Cortex *25*, 2574–2583.

66. Lindsley, D.B. (1939). A longitudinal study of the occipital alpha rhythm in normal children: frequency and amplitude standards. J. Genet. Psychol. *55*, 197–213.

67. Henry, C.E., and Greulich, W.W. (1944). Electroencephalograms of normal children. Monogr. Soc. Res. Child Dev. *9*, i–71.

68. Schaworonkow, N., and Voytek, B. (2021). Longitudinal changes in aperiodic and periodic activity in electrophysiological recordings in the first seven months of life. Dev. Cogn. Neurosci. *47*, 100895.

69. Suárez, L.E., Markello, R.D., Betzel, R.F., and Misic, B. (2020). Linking structure and function in macroscale brain networks. Trends Cogn. Sci. *24*, 302–315.

70. Vandewouw, M.M., Hunt, B.A.E., Ziolkowski, J., and Taylor, M.J. (2021). The developing relations between networks of cortical myelin and neurophysiological connectivity. Neuroimage *237*, 118142.

71. Rouder, J.N., and Morey, R.D. (2012). Default Bayes factors for model selection in regression. Multivariate Behav. Res. *47*, 877–903.

72. Parvizi, J., and Kastner, S. (2018). Promises and limitations of human intracranial electroencephalography. Nat. Neurosci. *21*, 474–483.

73. Faul, F., Erdfelder, E., Buchner, A., and Lang, A.G. (2009). Statistical power analyses using G*Power 3.1: tests for correlation and regression analyses. Behav. Res. Methods *41*, 1149–1160.

74. Oostenveld, R., Fries, P., Maris, E., and Schoffelen, J.M. (2011). FieldTrip: open source software for advanced analysis of MEG, EEG, and invasive electrophysiological data. Comput. Intell. Neurosci. *2011*, 156869.

75. Asano, E., Juhász, C., Shah, A., Sood, S., and Chugani, H.T. (2009). Role of subdural electrocorticography in prediction of long-term seizure outcome in epilepsy surgery. Brain *132*, 1038–1047.

76. Nakai, Y., Jeong, J.W., Brown, E.C., Rothermel, R., Kojima, K., Kambara, T., Shah, A., Mittal, S., Sood, S., and Asano, E. (2017). Three- and four-dimensional mapping of speech and language in patients with epilepsy. Brain *140*, 1351–1370.

77. Fischl, B. (2012). FreeSurfer. Neuroimage *62*, 774–781.

78. Pieters, T.A., Conner, C.R., and Tandon, N. (2013). Recursive grid partitioning on a cortical surface model: an optimized technique for the localization of implanted subdural electrodes. J. Neurosurg. *118*, 1086–1097.

79. Rossini, L., Garbelli, R., Gnatkovsky, V., Didato, G., Villani, F., Spreafico, R., Deleo, F., Lo Russo, G., Tringali, G., Gozzo, F., et al. (2017). Seizure activity per se does not induce tissue damage markers in human neocortical focal epilepsy. Ann. Neurol. *82*, 331–341.

80. Andersson, J.L.R., and Sotiropoulos, S.N. (2016). An integrated approach to correction for off-resonance effects and subject movement in diffusion MR imaging. Neuroimage *125*, 1063–1078.

81. Pierpaoli, C., Walker, L., Irfanoglu, M.O., Barnett, A., Basser, P., Chang, L.-C., Koay, C.G., Pajevic, S., Rohde, G., Sarlls, J., and Wu, M. (2010). TORTOISE: an integrated software package for processing of diffusion MRI data, *1597* (ISMRM 18th Annual Meet). https://archive.ismrm.org/2010/1597.html.

82. Tournier, J.-D., Calamante, F., and Connelly, A. (2010). Improved probabilistic streamlines tractography by 2nd order integration over fibre orientation distributions. Proc. Int. Soc. Magn. Reson. Med. *1670* https://archive.ismrm.org/2010/1670.html.

83. Smith, R.E., Tournier, J.D., Calamante, F., and Connelly, A. (2012). Anatomically-constrained tractography: improved diffusion MRI streamlines tractography through effective use of anatomical information. Neuroimage *62*, 1924–1938.

Please cite this article in press as: Johnson et al., Dissociable oscillatory theta signatures of memory formation in the developing brain, Current Biology (2022), https://doi.org/10.1016/j.cub.2022.01.053

84. Avants, B.B., Epstein, C.L., Grossman, M., and Gee, J.C. (2008). Symmetric diffeomorphic image registration with cross-correlation: evaluating automated labeling of elderly and neurodegenerative brain. Med. Image Anal. *12*, 26–41.

85. Garyfallidis, E., Brett, M., Correia, M.M., Williams, G.B., and Nimmo-Smith, I. (2012). QuickBundles, a method for tractography simplification. Front. Neurosci. *6*, 175.

86. Flinker, A., Korzeniewska, A., Shestyuk, A.Y., Franaszczuk, P.J., Dronkers, N.F., Knight, R.T., and Crone, N.E. (2015). Redefining the role of Broca's area in speech. Proc. Natl. Acad. Sci. USA *112*, 2871–2875.

87. Johnson, E.L., Dewar, C.D., Solbakk, A.-K., Endestad, T., Meling, T.R., and Knight, R.T. (2017). Bidirectional frontoparietal oscillatory systems support working memory. Curr. Biol. *27*, 1829–1835.e4.

88. Johnson, E.L., Adams, J.N., Solbakk, A.-K., Endestad, T., Larsson, P.G., Ivanovic, J., Meling, T.R., Lin, J.J., and Knight, R.T. (2018). Dynamic frontotemporal systems process space and time in working memory. PLoS Biol. *16*, e2004274.

89. Johnson, E.L., King-Stephens, D., Weber, P.B., Laxer, K.D., Lin, J.J., and Knight, R.T. (2018). Spectral imprints of working memory for everyday associations in the frontoparietal network. Front. Syst. Neurosci. *12*, 65.

90. Kam, J.W.Y., Helfrich, R.F., Solbakk, A.-K., Endestad, T., Larsson, P.G., Lin, J.J., and Knight, R.T. (2021). Top–down attentional modulation in human frontal cortex: differential engagement during external and internal attention. Cereb. Cortex *31*, 873–883.

91. Jones, K.T., Johnson, E.L., Tauxe, Z.S., and Rojas, D.C. (2020). Modulation of auditory gamma-band responses using transcranial electrical stimulation. J. Neurophysiol. *123*, 2504–2514.

92. Maris, E., Schoffelen, J.M., and Fries, P. (2007). Nonparametric statistical testing of coherence differences. J. Neurosci. Methods *163*, 161–175.

93. Maris, E. (2012). Statistical testing in electrophysiological studies. Psychophysiology *49*, 549–565.

94. Bastos, A.M., and Schoffelen, J.-M. (2016). A tutorial review of functional connectivity analysis methods and their interpretational pitfalls. Front. Syst. Neurosci. *9*, 175.

95. Baayen, R.H., Davidson, D.J., and Bates, D.M. (2008). Mixed-effects modeling with crossed random effects for subjects and items. J. Mem. Lang. *59*, 390–412.

96. Yu, Z., Guindani, M., Grieco, S.F., Chen, L., Holmes, T.C., and Xu, X. (2022). Beyond t test and ANOVA: applications of mixed-effects models for more rigorous statistical analysis in neuroscience research. Neuron *110*, 21–35.

97. Etz, A., Haaf, J.M., Rouder, J.N., and Vandekerckhove, J. (2018). Bayesian inference and testing any hypothesis you can specify. Adv. Methods Pract. Psychol. Sci. *1*, 281–295.

Please cite this article in press as: Johnson et al., Dissociable oscillatory theta signatures of memory formation in the developing brain, Current Biology (2022), https://doi.org/10.1016/j.cub.2022.01.053

STAR★METHODS

KEY RESOURCES TABLE

REAGENT or RESOURCE	SOURCE	IDENTIFIER
Deposited data		
Deidentified raw data	This paper	https://dx.doi.org/10.15154/1524240
Software and algorithms		
Custom-built MATLAB code	This paper	https://dx.doi.org/10.15154/1524240
MATLAB 2019b	MathWorks	https://mathworks.com
Psychtoolbox-3	Psychtoolbox	https://psychtoolbox.org
FieldTrip (release 20200422)	Oostenveld et al.[74]	https://fieldtriptoolbox.org
FreeSurfer software	FreeSurfer	https://surfer.nmr.mgh.harvard.edu
MRtrix3 toolbox	MRtrix3	https://www.mrtrix.org
Advanced Normalization Tools (ANTs)	ANTs	https://stnava.github.io/ANTs
JASP (0.14.1.0)	JASP Team	https://jasp-stats.org

RESOURCE AVAILABILITY

Lead contact

Further information and requests for resources should be directed to and will be fulfilled by the lead contact, E. L. Johnson (eljohnson@northwestern.edu).

Materials availability

This study did not generate new unique reagents.

Data and code availability

- Deidentified raw data have been deposited at the NIMH database and are publicly available as of the date of publication. The DOI is listed in the key resources table.
- All original code has been deposited at the NIMH database and is publicly available as of the date of publication. The DOI is listed in the key resources table.
- Any additional information required to reanalyze the data reported in this paper is available from the lead contact upon request.

EXPERIMENTAL MODEL AND SUBJECT DETAILS

Human subjects

Subjects were 21 children and adolescents (10 females and 11 males; 5.9-20.5 years of age; M ± SD, 13.5 ± 3.9 years) undergoing ECoG monitoring as part of clinical management of seizures at the Children's Hospital of Michigan. DWI data were obtained from 11 of these subjects (6 females; 6.2-16.7 years of age; M ± SD, 12.0 ± 3.2 years). Demographic details are provided in Table S1. Subjects were selected from a larger pool based on nonpathalogic coverage of MTL (i.e., electrodes localized to MTL and outsize seizure onset zones[75]) and there is partial overlap in subjects between this study and earlier studies using the same memory task.[42,43] Written informed consent was obtained from subjects aged 18 years and older and from the guardians of all subjects younger than 18 years; written assent was obtained from subjects aged 13-17 years and oral assent was obtained from younger children. The Wayne State University Institutional Review Board approved all procedures in accordance with the Declaration of Helsinki.

METHOD DETAILS

Memory task

Subjects performed a scene recognition memory task (Figure 1A) that has been used extensively to delineate the functional architecture of memory development with fMRI[14,18,44,46,47] and ECoG.[6,42,43] Subjects studied sets of 40 indoor and outdoor scenes,

Please cite this article in press as: Johnson et al., Dissociable oscillatory theta signatures of memory formation in the developing brain, Current Biology (2022), https://doi.org/10.1016/j.cub.2022.01.053

each shown for 3 s following a 0.5-s fixation interval. Stimuli were full-color pictures of natural scenes, half of high complexity and half of low complexity, characterized based on the number of object categories (over/under four) depicted.[43,45] Subjects were instructed to indicate verbally whether each studied item depicted an indoor or an outdoor scene. Responses were coded as correct or incorrect via offline review of individual audio recordings. A fixation cross remained on screen until a response was provided if none was provided during the 3-s scene presentation epoch. Per-trial RTs were automatically calculated by subtracting scene onset times from response onset times. Analysis of electrophysiological data was restricted to correct encoding trials—that is, trials in which scenes were correctly classified as indoor/outdoor, indicating the scenes were properly attended during the study block.[42,43]

The memory recognition test included all 40 scenes presented during the study block, intermixed in a randomized order with 20 new scenes. Each scene remained on screen until a response was given, following a 0.5-s fixation pretrial interval. Subjects were instructed to verbalize an old/new judgment of each scene, which was coded as a hit (correct old), miss (new response to an old scene), correct rejection (correct new), or false alarm (old response to a new scene) via offline review of individual audio recordings. Per-trial RTs were again automatically calculated by subtracting scene onset times from response onset times, and trials were excluded if no response was given. Study-test runs were administered in two consecutive cycles of 40 study scenes, followed by 40 studied + 20 new scenes. Half as many new scenes compared with previously studied scenes were introduced in the test phase so that the test remained engaging, and subjects overall responded old and new at roughly equal rates. All subjects completed a short practice run and at least one full study-test run.

Electrocorticography

Electrode placement and localization

Platinum macro-electrodes (10-mm intercontact distance, 4-mm diameter) were surgically implanted for extra-operative ECoG recording based solely on the clinical needs of each patient. Every patient in this study was implanted with an 8×8 electrode grid over lateral regions and strips over MTL (Figure S1B). Three-dimensional electrode reconstructions were created by co-registering post-implantation planar x-ray images of the cortical surface with preoperative T1-weighted spoiled gradient-echo magnetic resonance (MR) images.[76] Automatic parcellation of cortical gyri was performed using FreeSurfer software,[77] and electrode sites were assigned anatomical labels.[78] Subjects were selected by nonpathologic electrode placement in MTL (i.e., parahippocampal and rhinal cortices). Of the 21 subjects included in this investigation, 20 had electrodes recording simultaneously from PFC (same hemisphere). PFC electrodes were further classified into IFG, MFG, and SFG regions via group review of individual reconstructions and automatic parcellation results.[42] Electrodes were localized according to individual anatomy and transformed into standard Talairach space for visual representation across subjects (Figure 1C).

Data acquisition and preprocessing

ECoG data were acquired using a 192-channel Nihon Kohden Neurofax 1100A Digital System, sampled at 1 kHz. Raw electrophysiology data were filtered with 0.1-Hz high-pass and 300-Hz low-pass finite impulse response filters, and 60-Hz line noise harmonics were removed using discrete Fourier transform. Continuous study data were demeaned, epoched into 4.5-s trials (−1 to +3.5 s from scene onset), and manually inspected blind to electrode locations and experimental task parameters. Electrodes overlying seizure onset zones[75] and electrodes and epochs displaying epileptiform activity or artifactual signal (from poor contact, machine noise, etc.) were excluded. Every artifact-free electrode was referenced to the common average of all artifact-free electrodes. Data were manually re-inspected to reject any trials with residual noise. Preprocessing routines utilized functions from the FieldTrip toolbox for MATLAB.[74] All results are based on analysis of nonpathologic, artifact-free electrodes in regions of interest, ensuring that data represent healthy tissue.[79]

Structural imaging

Data acquisition and preprocessing

Diffusion-weighted images were acquired as part of preoperative structural MR imaging to visualize white matter pathways underlying electrode sites. T1-weighted images were collected using a GE Signa 3T scanner with an eight-channel head coil and array spatial sensitivity encoding technique (ASSET). For T1-weighted images, a fast-spoiled gradient echo sequence was applied at TR/TE/TI of 9.12/3.66/400 ms, outputting 1.2 mm slices at 0.94×0.94 mm^2 planar resolution. For diffusion-weighted images, a multi-slice, single-shot, diffusion-weighted echo-planar imaging sequence was applied at TR/TE of 12,500/88.7 ms with FOV = 24 cm. A 128×128 acquisition matrix at a nominal resolution of 1.89 mm with contiguous 3 mm slices covering the whole brain was obtained, outputting a single b = 0 (b0) image and 55 isotropic gradient directions with b = 1,000 s/mm^2. Diffusion-weighted images were corrected for motion, noise, and susceptibility- and eddy-induced distortions using FSL[80] and NIH TORTISE[81] packages. Three-dimensional reconstructions the whole brain were generated using FreeSurfer software.[77]

Inter-regional tractography

Streamline tractography utilized the second-order integration fiber orientation distribution (iFOD2) algorithm[82] of the MRtrix3 package. Regions of interest were defined by centering spheres of 5-mm radius on the Talairach-transformed coordinates of all MTL, IFG, MFG, and SFG electrodes. Outputs were combined within each region, mirrored across hemispheres, dilated and eroded by a neighborhood size of 20, and co-registered to the b0 diffusion space. Any overlapping voxels were assigned to the nearest electrode label. Within each patient's MTL region of interest, every voxel along the gray/white matter interface was seeded from 25,000 dynamically randomized points and streamlines terminating in IFG, MFG, and SFG were selected per anatomically constrained tractography.[83]

Please cite this article in press as: Johnson et al., Dissociable oscillatory theta signatures of memory formation in the developing brain, Current Biology (2022), https://doi.org/10.1016/j.cub.2022.01.053

Streamlines were normalized to the common FreeSurfer average space using a nonlinear warp field generated by the ANTs library package[84] and bundled into the cingulum or uncinate tract using the QuickBundles algorithm.[85] Spatial averages of these bundles yielded 12 bilateral pathway centroids representing exemplar MTL-IFG, MTL-MFG, and MTL-SFG connections, which were warped back to individual b0 diffusion space and resampled to 12 equidistant points to facilitate comparison. Streamlines were assigned to centroids with the minimum mean distance between corresponding resampled points. The pointwise distance z-score between streamlines and exemplars was then calculated and streamlines with mean, non-endpoint z-scores exceeding two standard deviations from exemplars were excluded. The resulting pathways were used as masks to weight FA values such that voxels with more streamlines more strongly influenced mean FA values.

QUANTIFICATION AND STATISTICAL ANALYSIS

Behavior

Based on performance at test, we calculated per subject the hit rate (i.e., number of previously studied scenes that were correctly recognized as old out of all studied scenes) and false alarm rate (number of new scenes presented at test that were incorrectly identified as old out of the number of new scenes presented at test). Recognition accuracy was calculated as hit rate minus false alarm rate to correct for differences in an individual's tendency to respond old or new.[18,42,43,46]

Spectral decomposition

Study data segments were zero-padded to 10 s to minimize filtering-induced edge artifacts and bandpass filtered at 30 logarithmically spaced, partially overlapping frequencies centered from 1.5 to 250 Hz (1/3 fractional bandwidth). The Hilbert transform was used to extract the analytic amplitude envelope from each filtered time series, which was squared to produce raw power values. We then extracted study data segments from −0.45 to +3 s for statistical analysis of event-related power in single trials. Power data were bootstrapped in single trials by standardizing the study data segments in the time domain. Raw power values were pooled into a single time series for each electrode and frequency, from which r data points (r = number of trials in that subject's dataset) were randomly selected and averaged. This step was repeated 1,000 times to create normal distributions of the study data. Raw power data were z-scored per time point on the distributions. This procedure adjusts the power outputs to correct for 1/f power scaling and reveals event-related spectral activity.[42,43,86–90]

Oscillatory peak detection

Irregular-resampling auto-spectral analysis (IRASA) was used to disentangle true oscillatory components from the aperiodic 1/f slope,[53] as implemented in FieldTrip.[57] Study data segments were epoched -0.45 to +3 s from scene onset, zero-padded, and analyzed from 1 to 20 Hz. The IRASA method compresses and expands the epoched data with non-integer resampling factors to redistribute oscillatory components while leaving the 1/f distribution intact. For each original and resampled data trace, the auto-spectrum was calculated using the fast Fourier transform after applying a Hanning window. The median was taken from the resampled auto-spectra to obtain the 1/f component for each electrode and subtracted from the original power spectrum to isolate oscillatory residuals. Peak detection was performed on the oscillatory residuals using a threshold of 4.5 Hz to distinguish slow from fast theta.[49–52]

Inter-regional amplitude coupling

Study data segments were zero-padded and bandpass filtered per-electrode at the theta peaks (1/3 fractional bandwidth) following removal of the ERP.[87–89,91] The filtered data were epoched from -0.45 to +3.5 s from scene onset and z-scored per trial in the time domain to control for differences in voltage between hit and miss trials. The Hilbert transform was used to extract the analytic amplitude envelope from each z-scored time series. Amplitude coupling was calculated between all MTL-PFC electrode pairs as time-shifted linear correlations independent of phase.[59] With this method, data subsegments are correlated across serial temporal lags (here, 0.5-s subsegments,[42] -0.1 to +0.1-s shifts) to indicate the strength and timing of inter-regional interactions. Calculations were performed at each timepoint separately on the means of hit and miss trials, and outputs were Fisher's Z-transformed.

Inter-regional phase coupling

Study data segments were zero-padded and bandpass filtered per-electrode at the theta peaks (1/3 fractional bandwidth) following removal of the ERP.[87–89,91] The filtered data were epoched from −were to +3 s from scene onset, and the Hilbert transform was used to extract instantaneous phase values from each filtered time series. Phase coupling was calculated between all MTL-PFC electrode pairs as phase-locking values independent of amplitude.[61] The PLV method calculates the consistency in electrode-pair phase differences across a series of data points. Calculations were performed at each timepoint separately across hit and miss trials, and statistical bootstrapping was used to control for mismatched trial counts. PLV data were bootstrapped in individual subjects by standardizing raw outputs against trial-shuffled surrogate distributions to control for differing numbers of hit and miss trials. At each electrode-pair, trials were randomly shuffled in one electrode and PLV was recalculated. This step was repeated 1,000 times to create normal distributions of surrogate PLV data. Raw PLV data were z-scored on the surrogate distributions. This procedure separately adjusts the hit and miss PLV outputs to correct for different numbers of hit and miss trials prior to analysis of subsequent memory effects.

Please cite this article in press as: Johnson et al., Dissociable oscillatory theta signatures of memory formation in the developing brain, Current Biology (2022), https://doi.org/10.1016/j.cub.2022.01.053

CellPress

Inter-regional phase-amplitude coupling

Study data segments were zero-padded and bandpass filtered per-electrode at the theta peaks (1/3 fractional bandwidth) and high-frequency band (70-150 Hz) following removal of the ERP.[87–89,91] The filtered data were epoched from −0.45 to +3 s from scene onset, and the Hilbert transform was used to extract the analytic amplitude envelope from the high-frequency time series. Then, the high-frequency data were bandpass filtered a second time at the theta peaks. The Hilbert transform was used to extract instantaneous phase values from both the theta and theta-filtered high-frequency time series. PAC was calculated between all MTL-PFC electrode pairs (PFC theta, MTL theta-filtered high-frequency) as phase-locking values independent of theta amplitude.[64] As in the analysis of phase coupling, PLV calculations were performed at each timepoint separately across hit and miss trials, and statistical bootstrapping was used to control for mismatched trial counts using the same method described above in the analysis of inter-regional phase coupling data.

Exploratory inter-regional analyses

Raw coherence (1.5-30 Hz) and PAC (PFC phase 1.5-30 Hz, MTL amplitude 30-250 Hz) were recomputed across all trials from the Hilbert-transformed data following removal of the ERP.[87–89,91] These data illustrate inter-regional interactions in the theta range across all electrode pairs without oscillatory peak detection or subsequent memory analysis (Figure S7).

Subsequent memory

Individually corrected power and functional connectivity data were tested for subsequent memory effects using Monte Carlo permutations with cluster-based correction for multiple comparisons.[48,92,93] Data were averaged per subject across electrodes within regions of interest separately for hit and miss trials, and subsequent memory effects were computed from the mean difference between hit and miss trials. This procedure avoids biasing the results to subjects with more electrodes.[90] Clusters were formed in time (and, for power, frequency) by thresholding paired differences at $p < 0.05$ using the maximum sum criterion. Permutation distributions were generated by randomly shuffling condition labels (1,000 iterations) and corrected p-values were obtained by comparing the observed data to the random permutation distributions. This is an extremely powerful approach because it recreates any biases in the data with each randomization and applies the maximum correction for multiple comparisons based on physiological constraints such as contiguous timepoints. Moreover, subsequent memory analysis serves to isolate signatures of memory formation while controlling for confounds shared across trials, such as spurious functional connectivity from common average referencing.[94] Subsequent memory effects are shown in Figures 2, 4B, 4C, 5B, 5C, S2, S6B, and S6D.

Inter-individual differences

Individual differences were investigated using linear mixed-effects models and Bayesian correlations. To investigate age-related differences in behavioral encoding and scene recognition performance, models included age as the fixed effect and subjects as random effects. To investigate individual differences related to age and recognition performance in peak frequencies, models included frequency (slow, fast), age, and performance as fixed effects, and subjects and nested electrodes as random effects. To investigate individual differences in subsequent memory effects and FA values, models included age and performance as fixed effects and subjects as random effects. Subsequent memory effects were averaged across data points within significant clusters and FA values were averaged bilaterally. By modeling subjects as random effects, these procedures control for shared variance in electrodes within a subject and differing numbers of electrodes across subjects.[42,43,88,90,95,96] A significant interaction of age and performance would indicate that a neural measure partially explains age-related differences in memory performance. The significance threshold for each measure was determined by Bonferroni correction. Interaction effects are shown in Figures 3C–3F, 6, 7A, and 7B.

However, because parametric statistics are vulnerable to sampling error, a non-significant model effect should not be considered evidence of a null effect.[71,97] This is particularly important given our sample size of 21, which, although relatively large for intracranial research,[72] is nonetheless small for analysis of inter-individual differences. Indeed, power analysis demonstrated that a sample of 21 subjects achieves >80% power ($\alpha = 0.05$, two-tailed) for a correlation of 0.55.[73] Less robust correlations, such as known positive relationships between age and performance on this task,[6,14,18,42–45] would therefore not achieve sufficient power using traditional p-values. Neither would correlations based on smaller samples, such as function-structure mapping in the DWI sample of 11 subjects. For these reasons, we utilized Bayesian correlations to disentangle subthreshold hypothesized effects from null effects.[93] The Bayes Factor (BF) quantifies both hypothesized and null effects, with $BF_{10} > 10$, $BF_{10} > 3$, and $BF_{10} > 1$ representing strong, modest, and anecdotal evidence of the hypothesized effect and $BF_{10} < 1/10$, $BF_{10} < 1/3$, and $BF_{10} < 1$ representing strong, modest, and anecdotal evidence of the null effect. Bayesian correlations were performed using the open-source JASP software with the default prior of 1. Bayesian correlations are shown in Figures 1B, 7C, and 7D.